#### **TOPICAL REVIEW**

### Mirror twin grain boundaries in molybdenum dichalcogenides

To cite this article: Matthias Batzill 2018 J. Phys.: Condens. Matter 30 493001

View the article online for updates and enhancements.



## IOP ebooks™

Bringing you innovative digital publishing with leading voices to create your essential collection of books in STEM research.

Start exploring the collection - download the first chapter of every title for free.

#### https://doi.org/10.1088/1361-648X/aae9cf

#### **Topical Review**

# Mirror twin grain boundaries in molybdenum dichalcogenides

#### 

Department of Physics, University of South Florida, Tampa, FL 33620, United States of America

E-mail: mbatzill@usf.edu

Received 31 July 2018, revised 10 October 2018 Accepted for publication 19 October 2018 Published 20 November 2018



#### **Abstract**

Mirror twin grain boundaries (MTBs) exist at the interface between two grains of 60° rotated hexagonal transition metal dichalcogenides (TMDC). These grain boundaries form a regular atomic structure that extends in one dimension and thus may be described as a onedimensional (1D) lattice embedded in the 2D TMDC. In this review, the different atomic structures and compositions of these MTBs are discussed. The obvious formation of MTBs is by coalescence of two twinned grains. In addition, however, in MoSe<sub>2</sub> and MoTe<sub>2</sub> a different formation mechanism has been revealed for the formation of Mo-rich MTBs. It has been shown that excess Mo can be incorporated into the TMDC lattices. These excess Mo atoms can then reorganize into closed, triangular MTB-loops that can grow in size by adding more Mo atoms to them. This mechanism allows the formation of dense MTB networks in MoSe<sub>2</sub> and MoTe2. Such MTB networks have been observed in samples grown by molecular beam epitaxy (MBE) and consequently their presence needs to be considered in understanding the properties of MBE grown MoSe<sub>2</sub> and MoTe<sub>2</sub>. Density functional theory as well as photoemission spectroscopy of MTB networks have shown that MTBs exhibit dispersing 1D-bands that intersect the Fermi-level, thus suggesting that these are 1D electron systems. Consequently, experimental data have been interpreted to reveal a charge density wave (or Peierls) instability, as well as a Tomonaga-Luttinger liquid behavior for electrons confined in 1D. We discuss these observations and the controversies that remain in the interpretation of some data. The metallic properties of the MTBs and their formation in dense networks also sparked the potential use of such crystal modifications for making metallic contacts to MoTe<sub>2</sub> or MoSe<sub>2</sub>. Moreover, these crystal modifications may also boost the catalytic properties of these materials.

Keywords: grain boundaries, molecular beam epitaxy, transition metal dichalcogenides, Tomonaga-Luttinger liquid, line defects, metallization, 1D metal

(Some figures may appear in colour only in the online journal)

In bulk materials, grain boundaries are extended planar defects. In 2D materials, however, grain boundaries between two rotated (or twisted) grains become 1D line defects. Mirror twin grain boundaries (MTBs) are special low symmetry grain boundaries that can be described by mirroring the crystal structure, with the grain boundary representing the mirror-line. MTBs in transition metal dichalcogenides (TMDCs)

originate from the three-fold (120°) symmetry of the monolayers. Thus, two mirrored grains are equivalent to two grains rotated by 60° and will form a MTB. The two grains can be 'stitched' together along the boundary in different structures and with varying compositions. Compositional and structural variations give rise to electronic states that lie within the band gap of the  $MoX_2$  host material and can form dispersing one

dimensional (1D) bands. Dispersing bands are not observed in other (twist) grain boundaries, which mostly exhibit localized band gap states, and this makes MTBs special in their properties. Having dispersing bands that intersect the Fermi-level would make MTBs 1D electron systems and we will discuss evidence for 1D-electron behavior in these MTBs. Related to MTBs are edges of monolayer islands that may also exhibit metallic states and that have been studied extensively for MoS<sub>2</sub> [1]. The electronic and chemical properties depend on the edge termination [2, 3] and because of the importance of MoS<sub>2</sub> in (electro)catalysis [4] these edges have been studied in particular in view of their catalytic properties [5, 6]. In contrast to edges, MTBs are entirely embedded within a 2D sheet of a TMDC and there are no free edges. Similar to edges MTBs may exhibit compositional variations and thus some of the properties of MTBs may be related to those of edges. However, in this review, we focus on embedded grain boundaries, only.

In this review, we are also interested in the formation processes of MTBs. While coalescence of grains rotated by 60° is an obvious process, there are other ways by which closed twin-grain boundary loops may form within a monolayer. Related to the compositional variation of MTBs, we show that in some TMDCs grain boundary loops form by condensing excess metal atoms into metal rich twin boundaries. This formation mechanism is another special property of MTBs compared to grain boundaries with different twist angles that cannot form by a nucleation and growth process and thus 'regular' twist grain boundaries are exclusively formed by the coalescence of rotated grains. Formation of MTB loops by incorporation of excess Mo into the lattice, appears to be an important defect formation process during synthesis of MoSe<sub>2</sub> and MoTe<sub>2</sub> mono- and few layers, especially in molecular beam epitaxy (MBE). Thus, understanding of these formation mechanisms are crucially important for improving the direct growth of TMDCs, especially for making van der Waals (vdW) heterostructures by direct growth methods. While the easy exfoliation and stacking of many vdW materials often enables rapid study of vdW heterostructures in academic research laboratories [7-22], clearly for a relevant technology the direct growth of these materials needs to be explored [23, 24]. Direct growth [25-41] is generally explored by chemical vapor deposition (CVD) [42, 43] or MBE [44-46]. For the growth of well-defined single layer heterostructures, MBE should enable better growth conditions. Indeed the use of MBE has been explored already in the 1990s for the growth of van der Waals (vdW) materials [47-59] Growth of vdW hetero-materials on vdW substrates has been dubbed 'van der Waals epitaxy'. In this growth mode the film is rotationally aligned with the substrate, although the lattices of film and substrate are mismatched. The lattice mismatch causes the formation of long range moiré structures. Thus this growth of rotational alignment vdW films on single crystalline vdW substrates, enables the synthesis of single crystalline mono- to few-layer materials. The weak interlayer interaction between the substrate and the film promises the formation of large scale vdW heterostructures. Rotationally aligned growth of vdW materials is commonly observed and verified by

diffraction, e.g. electron diffraction (LEED or RHEED) [60], or by obtaining angle resolved photoemission spectroscopy (ARPES) data of the *k*-space resolved electronic structure on single layer vdW materials grown on vdW substrates [61–64]. However, such space averaging techniques are not able to detect potential point- and line-defects in these materials. For (opto)electronic applications such defects can be detrimental as they may induce gap states that can cause localized charge carrier states in transport measurements [65, 66] or charge trap and recombination sites for optically excited charge carriers [67]. On the other hand, defects can have desirable chemical functionalities [68] and controlled formation of specific defects may enable the design of chemical sensors or catalysts.

Herein, we focus on the Mo-dichalcogenide family, which includes MoS<sub>2</sub>, MoSe<sub>2</sub>, and MoTe<sub>2</sub>. Only the 2H-polymorph, i.e. the trigonal prismatic crystal structure, is considered. We mainly focus on MTBs formed in MBE grown monolayers on vdW substrates. But mirror twin grain boundaries have also been observed in CVD grown samples [69] and formed by electron-beam induced defect formation in a transmission electron microscope [70]. The goal is to highlight challenges for the direct growth of Mo-dichalcogenides and their vdW heterostructures. On the other hand we discuss the interesting electronic and chemical properties MTBs in Mo-dichalcogenides possess and therefore the controlled formation of such MTBs may enable the design of a new class of materials.

#### 1. Classification of MTBs

The hexagonal prismatic  $MoX_2$  (X=S, Se, or Te) structure has a  $120^\circ$  in-plane rotational symmetry. Thus rotation of the hexagonal lattice by  $60^\circ$  does not reproduce the original lattice, but rather results in a mirrored structure as is illustrated in figure 1. If such two mirror grains coalesce they cannot be 'stitched' together into a perfect lattice but instead a grain boundary is formed, which we call a MTB. For 2D materials a grain boundary is always a line-defect. There exist more than one way to stitch the lattices of the two mirror-twin grains together, that differ in their formation energy and their composition. Various grain boundaries have been simulated by DFT and these are summarized next before we discuss experimentally observed structures.

#### 1.1. Computationally assessed MTBs

Figure 1 shows ball-and-stick models of possible MTBs [71] and their formation energies [72]. We may distinguish grain boundaries, which connect either two MoX<sub>2</sub> half-lattices that are terminated by chalcogens (labeled Se-edge in figure 1(a)) or half-lattices that are terminated by Mo-atoms (labeled Mo-edge in figure 1(a)). The grain boundaries that connect these two half-lattices, generally deviate from the MX<sub>2</sub> composition. Those connecting Se-edge terminate half-lattices are Mo-rich and those that are connecting Mo-edge terminated half-lattices are Se-rich. Because of the non-stoichiometry of the grain boundary the formation energies of the grain

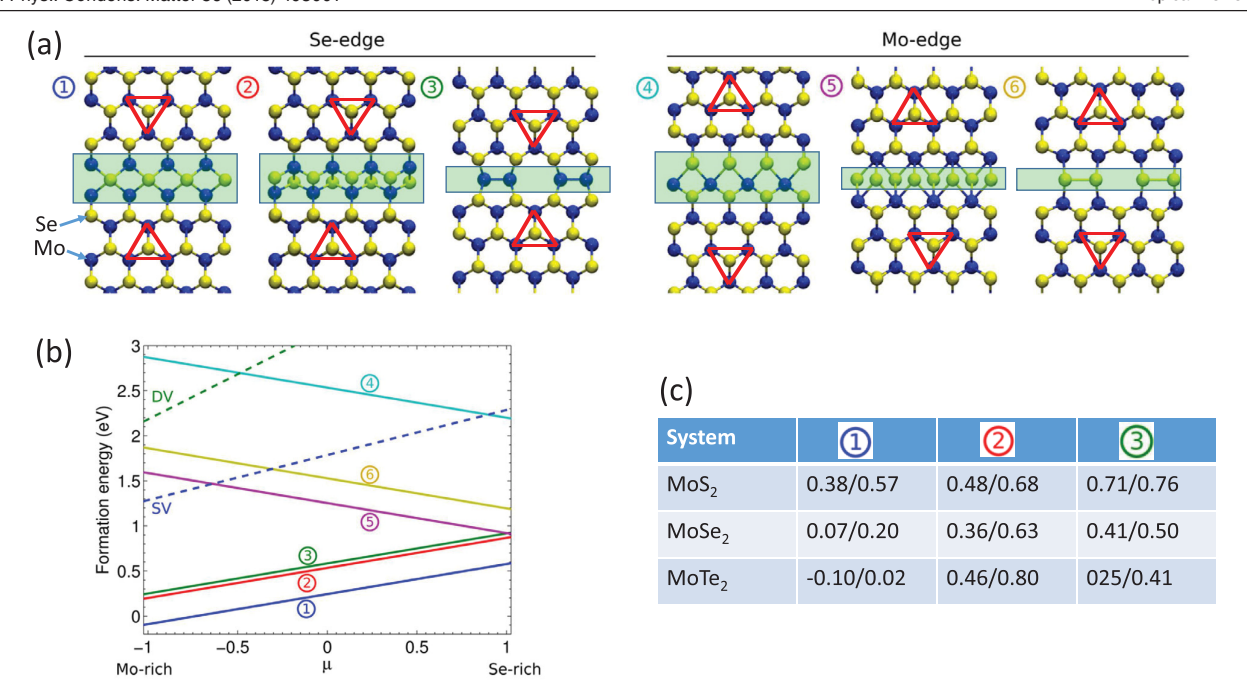


Figure 1. Various structures and corresponding formation energies computed for MTBs in 2H Mo-dichalcogenides. Structural models for MTBs are shown in (a), where the red triangle indicates the mirroring of the top lattice with respect to the bottom lattice. The green-shaded area indicates the grain boundary that is inserted between the two stoichiometric half-lattices. The composition of the grain boundaries varies for the different structures and in general is not stoichiometric, i.e. not  $MoX_2$ . All the structures that are formed when the half-lattices have Se-edges are Mo-rich (structure 1 and 2, shown in figure have a Mo:Se ratio of 1:1 for the green shaded area), while the grain boundaries that form with Mo-edge termination of the half-lattices are Se-rich. As a consequence of the non-stoichiometry of the grain boundaries, the formation energies are dependent on the selenium chemical potential as shown in (b) for  $MoS_2$ . A comparison of the formation energies for different Mo-dichalcogenides is shown in (c). The energies are in eV and shown for the three Mo-rich MTB structure (the Se-rich structures 4, 5, and 6 that have high formation energies as shown in (b) have not again been systematically considered in (c)). The two values correspond to the case when the lateral direction is allowed to relax and when the edges of the ribbon are fixed in the calculations. (a), (b) Reprinted with permission from [71]. Copyright (2015) American Chemical Society.

boundaries become dependent on the chemical potential of the components. From figure 1(b), it can be seen that the formation energy of the Mo-rich grain boundaries for MoSe<sub>2</sub> is always lower than that of Se-rich grain boundaries independent of the chemical potential. This suggest that the grain boundaries that can be experimentally obtained should be of the Mo-rich (Se-edge in figure 1(a)) kind. A comparison of the formation energies of the three Mo-rich MTBs for the three Mo-dichalcogenides are shown in the figure 1(c). Apart from structure 2, which exhibits fairly comparable formation energies for the three different MX<sub>2</sub>, the formation energies are much lower in MoTe2 than MoSe2 and highest in MoS2 for structures 1 and 3. This suggest that MTB formation occurs most readily in MoTe<sub>2</sub> and the least in MoS<sub>2</sub>. Also in all three systems, structure 1 has the lowest formation energy and thus should be the most common. However, under growth conditions and formation by atom-removal from a lattice, the ability for the lattice to relax as well as kinetic barriers may play an important role in defect formation in addition to these thermodynamic considerations. It also should be pointed out that although the structures shown in figure 1 are likely the lowest energy configuration, this is not an exhaustive list and other structures may be constructed. For example a 4 | 8 line defect,

i.e. a line defect that has a four-membered and eight-membered ring as the repeat unit, can be constructed as shown e.g. in [69].

#### 1.2. Experimentally observed MTBs

Transmission electron microscopy has been used to image MTBs in various TMDCs [69, 71, 73, 74]. To the best of our knowledge only chalcogen-deficient MTBs have been observed. This is consistent with the lower formation energies of such defects as discussed in the previous sub-section. Figure 2 shows TEM images of MTBs corresponding to structures 1 to 3 in figure 1.

The MTBs in these samples may have different origins. Either they are formed in monolayer growth by CVD or MBE, or in some cases their formation has been observed as a consequence of electron beam damage during imaging with the TEM [70, 71]. The high energetic electron beam in a TEM may knock-out chalcogen atoms that then can rearrange into MTB-loops. This process causes the formation of an inversion domain (lattice rotated by 60°) that is bound by a Mo-rich MTB. The formation of such an MTB-loop under e-beam irradiation is shown in figure 3.

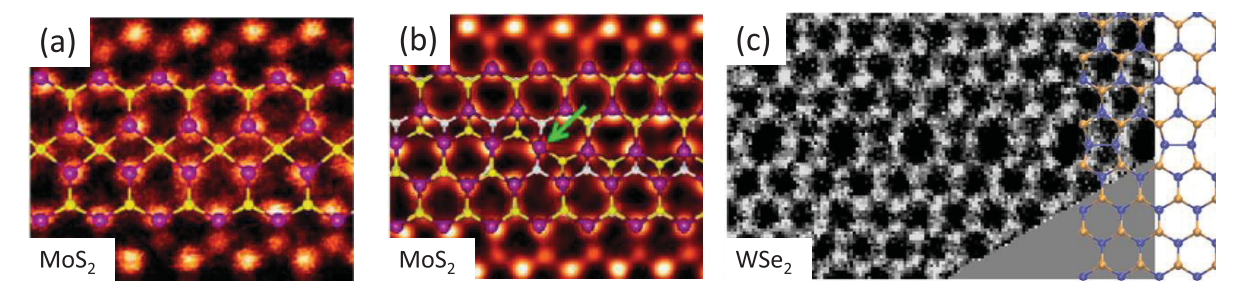


**Figure 2.** MTBs observed in TEM. The three MTBs that have been identified in TEM images of TMDs are chalcogen deficient and are those identified in figure 1 to have the lowest formation energies. (a) and (b) are MTBs observed in CVD-grown MoS<sub>2</sub>. While 55 | 8 structure (i.e. repeat unit of two 5-fold rings and one 8-fold ring) has been observed in WSe<sub>2</sub>. (a), (b) Reprinted with permission from [69]. Copyright (2017) American Chemical Society. (c) Reproduced from [73]. CC BY 4.0.

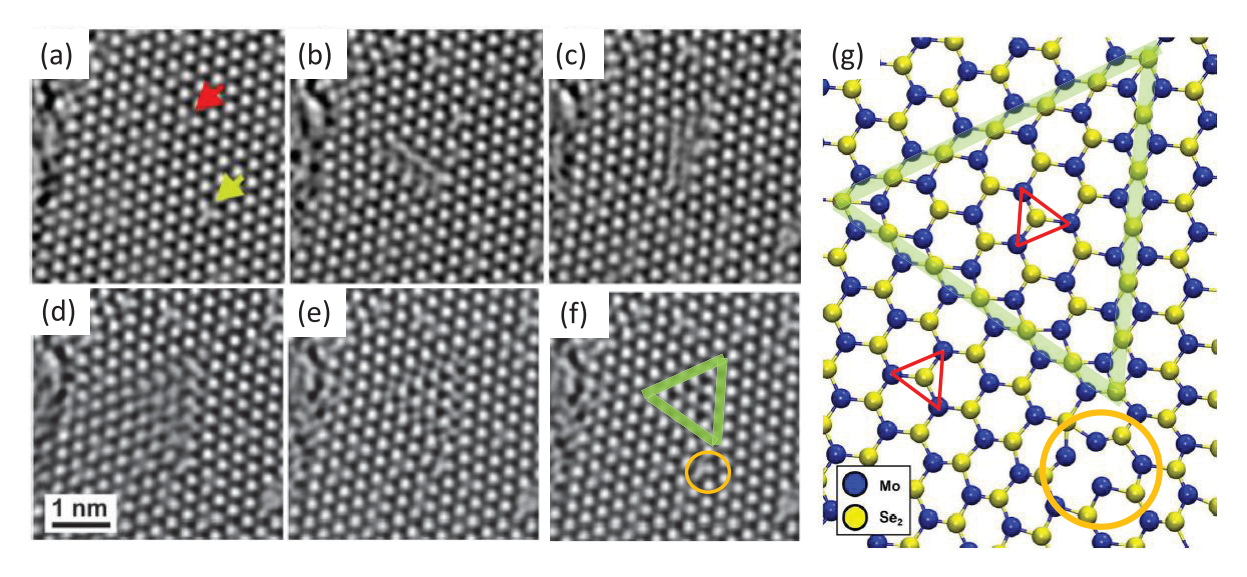


**Figure 3.** Formation of an MTB-loop in  $MoSe_2$  monolayers under e-beam irradiation in a TEM. Images (a)–(e) is a time sequence of the evolution of the crystal as Se-atoms are removed. In (e) a triangular MTB-loop is observed, which is highlighted in (f) by the green lines. In addition a dislocation core is also observed, highlighted by the orange circle. The corresponding atomic structure is shown in (g) as a ball-and-stick model. Reprinted with permission from [71]. Copyright (2015) American Chemical Society.

## 2. Formation mechanisms for MTBs during vdW epitaxy

Growth of TMDs on dissimilar hexagonal vdW substrates usually results in rotationally aligned growth of the film with respect to the substrate, i.e so-called vdW epitaxy. However, if the substrate has a higher symmetry than the TMD film we may expect the nucleation of equivalent TMD domains that are rotated. For instance if graphene is used as a growth substrate, then there is no difference in the coordination of two TMD grains rotated by 60° with respect to the substrate. Consequently if such rotated domains coalesce, a MTB has to form, as illustrated in figure 4. This implies that MTBs are naturally formed on hexagonal substrates that have 60° rotational symmetry rather than the 120° symmetry of the TMDs. Formation of such grain boundaries can be, for example, seen for MoS<sub>2</sub> grown on graphene/Ir(111) as shown in the scanning tunneling microscopy (STM) images of monolayer islands of MoS<sub>2</sub> formed by the coalescence of different islands [75]. In these images, the grain boundaries appear bright, which is a consequence of their metallic nature as is discussed below. Two kinds of MTBs are observed in these MoS<sub>2</sub> films that likely correspond to structure 1 and 2 in figure 1.

To avoid formation of mirror twin domains (60° rotation grains) due to the nucleation of equivalent rotated grains a substrate with the same symmetry is required. Such substrates may be another TMD or a (111) face of a fcc-metal. Still, even on these substrates the formation of mirror domains may be quite prevalent because the difference in the adsorption energies of the two 60° rotated domains may be very small. Thus single orientations may only be obtained by carefully characterizing and tuning of the growth conditions. This has been demonstrated for the growth of  $MoS_2$  on Au(111), where only under the right growth conditions a single orientation was preferred and otherwise twin domains were observed [76]. Thus for MoS<sub>2</sub>, films with a low density of inversion domains and consequently MTBs can be grown by MBE. Avoiding MTBs appears to be more challenging for MoSe<sub>2</sub> and MoTe<sub>2</sub> for which high densities of MTB-networks have been frequently

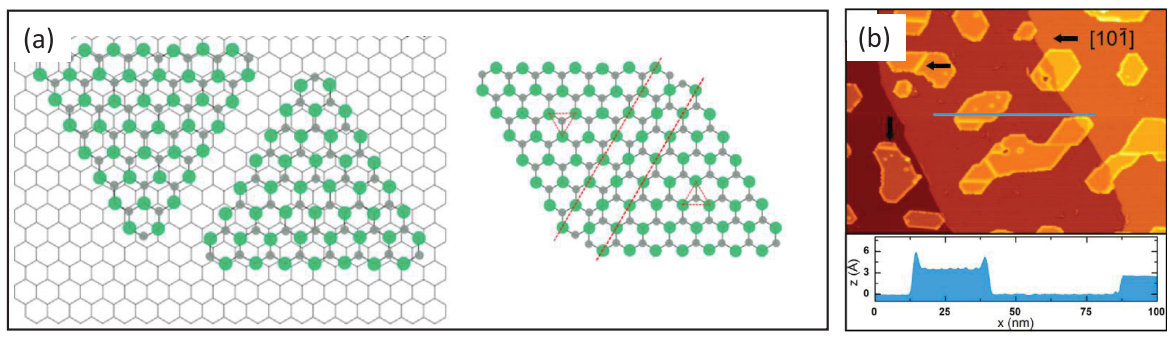


**Figure 4.** In vdW epitaxy of TMDs on graphene two equivalent orientations of TMDs rotated 60° relative to each other exist. If these grains coalesce, a MTB is formed as schematically illustrated in (a). Such MTBs are for instance observed for MoS<sub>2</sub> grown on graphene. In (b) STM images of monolayer islands on graphene/Ir(111) show straight bright lines that are identified as metallic MTBs. The line profile also shows the bright metallic edges of the MoS<sub>2</sub> islands. (b) Reproduced from [75]. © IOP Publishing Ltd. All rights reserved.

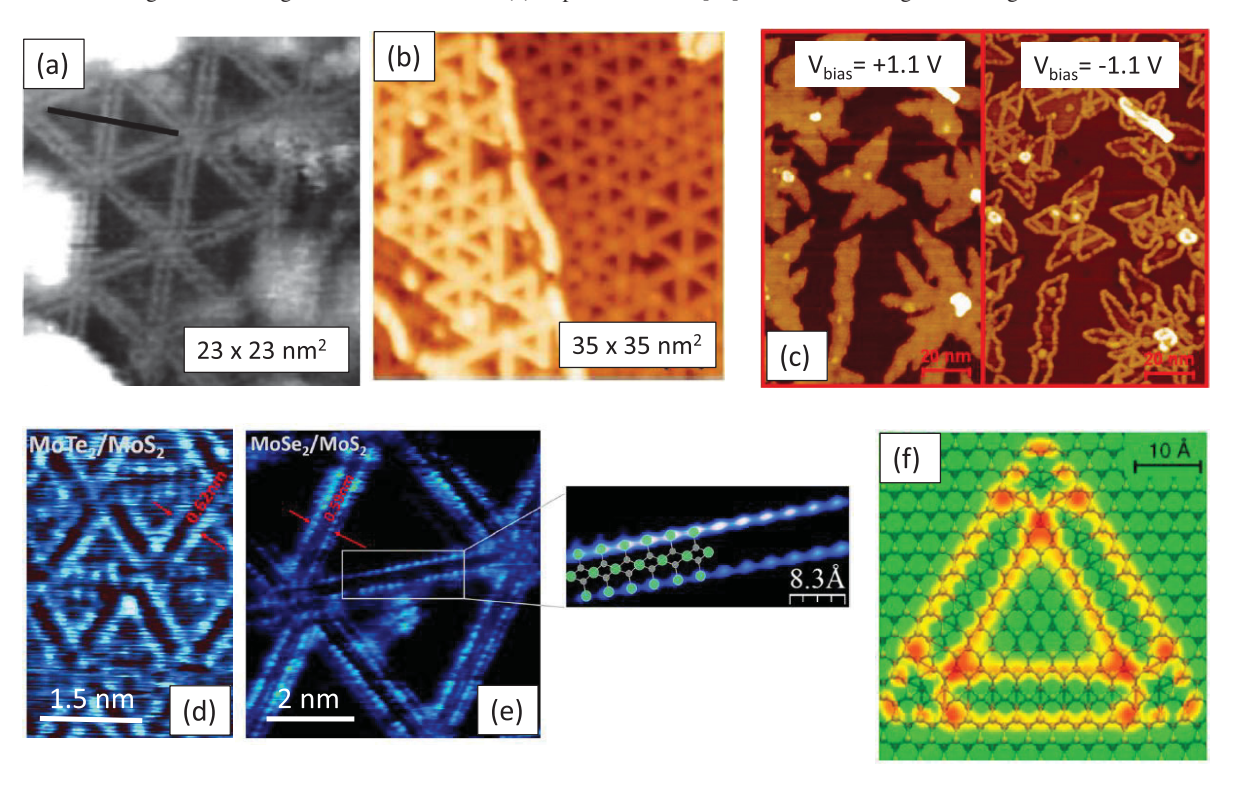


**Figure 5.** STM observations of MTB-networks in MBE-grown MoSe<sub>2</sub> and MoTe<sub>2</sub>. MoSe<sub>2</sub> grown on MoS<sub>2</sub> substrate (a) or HOPG substrate (b). In STM, the line defects appear brighter than defect free material for negative bias voltages (tunneling into filled states). This enhanced contrast of the line defects can be seen in (c) for the case of MoSe<sub>2</sub> islands on a MoS<sub>2</sub> substrate. The island edges also appear brighter, suggesting that they have similar electronic states in the band gap as the line defects. An even higher density of line defects is observed in MoTe<sub>2</sub> as shown in (d) compared to MoSe<sub>2</sub> shown in (e) under similar growth conditions. MTBs in MoSe<sub>2</sub> and MoTe<sub>2</sub> are imaged as two bright rows in high-resolution STM as illustrated in (e) for a filled state image taken at room temperature. This STM contrast is consistent with simulated STM image for a triangular MTB loop shown in (f) for a type-1 (according to classification in figure 1) MTB. (a) Reprinted with permission from [77], copyright (1999) by the American Physical Society. (b) Reprinted with permission from [78], copyright (2014) by the American Physical Society. (c) Reprinted with permission from [86]. Copyright (2018) American Chemical Society.

observed in MBE grown monolayer materials. Koma, an early pioneer of vdW epitaxy, observed modulated patterns in STM images of MBE-grown MoSe<sub>2</sub> monolayers on MoS<sub>2</sub> substrates already in the late 1990s as shown in figure 5(a) [77]. However, we know now that this was interpreted wrongly as a moiré pattern. In 2014 Liu *et al* observed the same line patterns on MBE-grown MoSe<sub>2</sub> on HOPG (figure 5(b)) and they

interpreted, assisted by high resolution TEM, these lines correctly as MTBs (however, they incorrectly interpreted their TEM images and suggested the Mo was in the center of the MTB rather than Se, i.e. in the scheme of figure 1, they suggested structure 4 rather than the correct structure 1) [78]. The MTBs in MoSe<sub>2</sub> appear as bright lines for filled state images and far less pronounced in empty state images as illustrated

in figure 5(c) [79]. The strong dependence of the contrast on the imaging conditions indicates the electronic origin of the apparent height in STM micrographs. Similar line defect networks were observed in other reports of MBE grown MoSe<sub>2</sub> [38, 80–82] figures 5(d) and (e) shows that even denser MTB networks are observed in MoTe<sub>2</sub> compared to MoSe<sub>2</sub> under similar growth conditions [83–85] MTBs are imaged as double rows in high resolution STM and atomic corrugation is observed for positions of the Se-atoms adjacent to the MTB-core as is shown in figure 5(e), which is consistent with simulated STM images shown in figure 5(f) [86].

Clearly, formation of such high densities of MTB networks are not likely to form by the coalescence of 60° degree rotated grains as is suggested to be the mechanism for MoS<sub>2</sub>. We already have seen above from TEM experiments that changes in the composition of the MoSe<sub>2</sub> sheet can result in a restructuring into MTB-loops [69, 70] Since the lowest energy MTB structures are chalcogen deficient (or equivalently, Mo enriched) it could be considered that mechanisms exist that causes formation of such MTBs by modifying the composition during growth. For instance at higher temperatures, chalcogens may desorb and the ensuing chalcogen deficiency (if not replenished by the chalcogen molecular beam) could cause a rearrangement into energetically favorable grain boundary networks rather than forming other defects such as vacancies. To test this hypothesis one may for example anneal a single crystal sample in vacuum. For MoTe2, vacuum annealing to 400 °C indeed has shown to result in Te-loss induced formation of MTB networks [87]. This would indicate that lower growth temperatures are required for MoTe2, however, in many MBE growth experiments the temperatures are less (~300 °C). Moreover, while MoTe<sub>2</sub> is prone to loose Te, MoSe<sub>2</sub> is significantly more stable and significant Se-loss should occur at higher temperatures. Consequently, additional mechanisms are likely to contribute to the formation of MTBs. Assuming that non-stoichiometry of the sample is crucial for the formation of MTB networks in MoSe<sub>2</sub> and MoTe<sub>2</sub> one may consider to add excess Mo to the growing layer. During MBE growth the sample is constantly exposed to a flux of atomic Mo (and chalcogens), thus if the atomic Mo species can incorporate into the MX2 lattice the surface would become Mo enriched which then may result in restructuring into MTBs. To test this hypothesis, single crystal MoX<sub>2</sub> samples were exposed to a pure Mo-beam (with a very low flux) [86] with the sample held at a typical MBE growth temperature of 350 °C. Figure 6 shows a comparison of the surface structure of the three different Mo-dichalcogenides for increasing Mo-exposure. Clear differences in the formation of MTBs on the different materials are observed. On MoTe<sub>2</sub> MTBs seem to form readily and the high density (even for incomplete coverage) suggest that there is a low barrier for nucleating MTB-loops. In MoTe<sub>2</sub> very high densities can be obtained with at least 10% of excess Mo incorporated into the surface layer of MoTe<sub>2</sub>. Such a dense network with high Mo-excess may qualify this material as a new phase of  $MoTe_{2-x}$  material, comparable to the wellknown Ti-rich Magnéli phases in reduced rutile  $TiO_{2-x}$  [88] In MoSe<sub>2</sub>, MTB formation is also observed for lower excess Mo-concentrations. However, larger triangular MTB-loops are observed, which may be a consequence of higher nucleation barriers and rather than nucleating new MTBs it is easier to grow existing MTBs by incorporating Mo. Moreover, the total achievable coverage of MTBs on MoSe2 with this approach seems limited and eventually Mo prefers to form ad-clusters at the surface rather than being incorporated into MTBs. In contrast to MoTe2 and MoSe2, no MTB-loops are observed in MoS<sub>2</sub>. The difference in the formation of MTBs seem to correlate well with the computed formation energies for type-1 MTBs for the different MoX<sub>2</sub>, summarized in figure 1(c). In particular the very low (or even negative) formation energy of MTBs in MoTe<sub>2</sub> seems to agree with the easy formation in the presence of excess Mo. These studies suggest that incorporation of excess Mo in MoTe2 and MoSe2 during MBE growth may be responsible for the formation of MTB-loops in these materials, while no such defects are expected to readily form

To understand the mechanism of incorporation of excess Mo into the MoX<sub>2</sub> lattices better, detailed DFT simulations were performed [86] and the main results are presented in figure 7. A single excess Mo-atom has the lowest energy in split interstitial sites for MoS2 and MoSe2, while the interstitial site is preferred for MoTe<sub>2</sub> (see figure 7(a)). This changes for two excess Mo-atoms. In that case an adsorbed Mo-dimer is the lowest energy configuration for  $MoS_2$  (see figure 7(b), and this may be the reason why on MoS2 Mo ad-clusters are observed rather than incorporation of Mo into the lattice. In contrast, for both MoSe<sub>2</sub> and MoTe<sub>2</sub> the incorporation of two excess Mo-atoms in adjacent interstitial sites becomes the most energetically favored configuration. Adding one more Mo-atom, i.e. a total of three excess Mo atoms, one starts seeing the formation of a triangular MTB-loop as illustrated in figure 7(c). The restructuring of the lattice by adding another Mo-atom, i.e. a total of four excess Mo-atoms, is illustrated in figure 7(d). Figure 7(d) suggests a possible mechanism for the growth of a MTB loop, the individual steps and the corresponding formation energies at different stages of the expansion of the MTB-loop are calculated, indicating that the process is energetically downhill.

Thus in addition to the coalescence of 60° rotated grains, MTBs in MoSe<sub>2</sub> and MoTe<sub>2</sub> can also be formed by introducing Mo-enrichment. This may be achieved by removal of chalcogens, for instance by e-beam damage or thermal sublimation of chalcogens, or by addition of Mo, for instance by vapor deposition of Mo. Especially in MoTe<sub>2</sub> this can result in very dense MTB networks, with up to 10% excess Mo incorporated in these MTBs. While this easy incorporation of Mo presents a challenge for growing defect free MoSe<sub>2</sub> and MoTe<sub>2</sub>, it may also present opportunities to modify the materials to obtain new properties. In the following we discuss the electronic properties of these MTBs.

#### 3. Electronic properties of MTBs

The electronic structure of the type 1 MTB (according to figure 1) has been calculated for MoS<sub>2</sub> [89, 90] and MoSe<sub>2</sub> [71] by DFT and shows for both cases strongly-dispersing

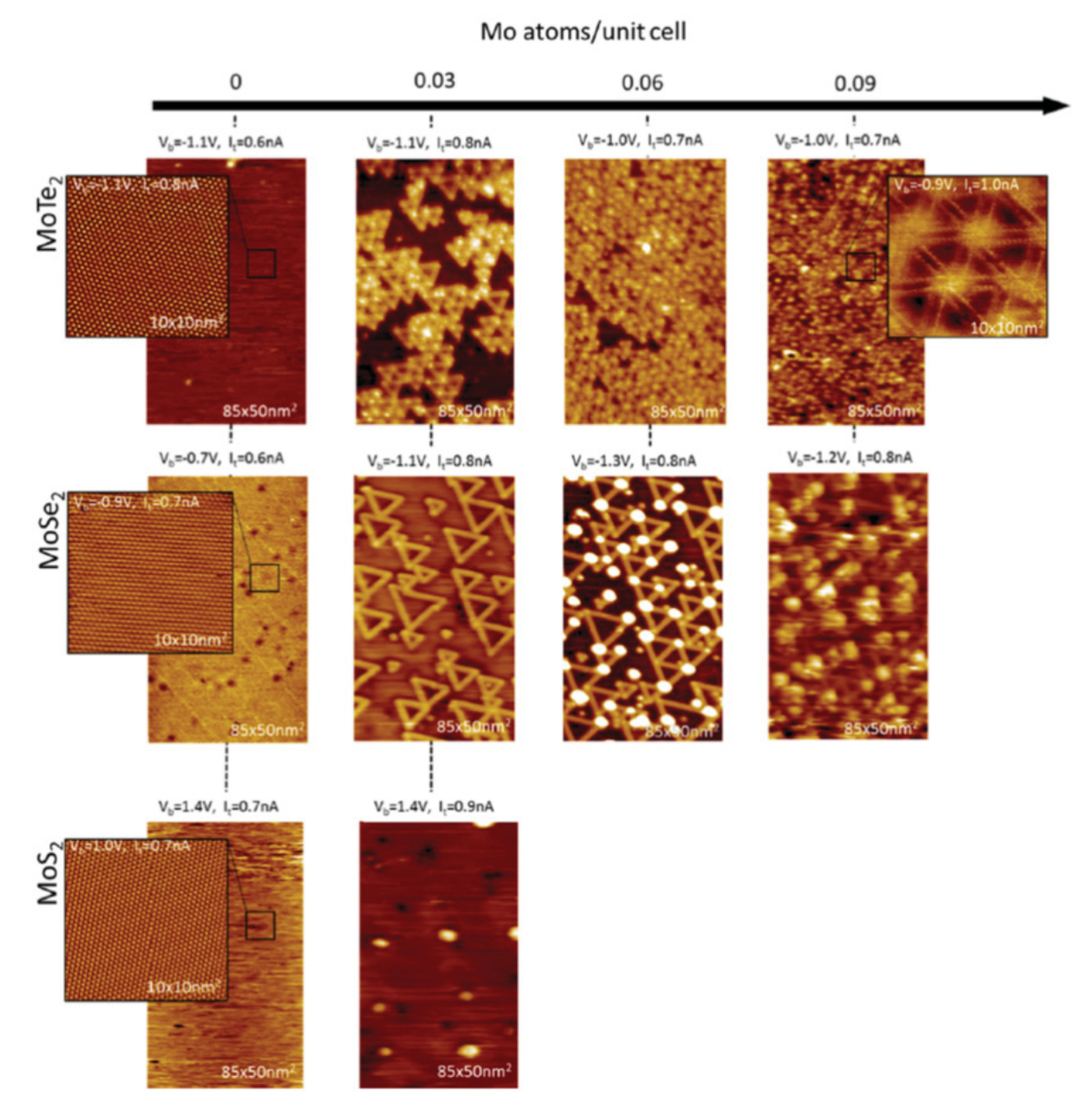


Figure 6. Surface evolution of single crystal  $MoX_2$  with increasing exposure to a Mo flux and the sample at 350 °C. The pristine substrates do not exhibit any line defects. In  $MoTe_2$  (top row) exposure to Mo causes the formation of dense networks of MTBs that increases with increasing Mo deposition allowing absorption of ~10% excess Mo into the crystal structure. For  $MoSe_2$  (middle row), larger triangular MTB loops are formed initially, but eventually Mo-clusters are observed that preferentially nucleate in the corners of the triangular MTB-loops. For  $MoSe_2$  (bottom row) no MTBs are observed, instead Mo-cluster formation is observed already for the lowest Mo-exposure. Reprinted with permission from [86]. Copyright (2018) American Chemical Society.

metallic-bands within the band gap of the MoX<sub>2</sub>. This is remarkable since most other twist grain boundaries in these materials mostly exhibit strongly localized gap states [89] and so do 55 | 8 grain boundaries in graphene [91]. Moreover, since grain boundaries in 2D materials are line defects, the electronic properties should be 1D. Importantly, the dispersing defect states are predicted by DFT and shown below by ARPES, to lie entirely within the forbidden energy gaps of the host material. This implies that these states cannot couple to the electronic states of the 2D host and thus are electronically

confined to the 1D defect, making them ideal 1D systems. There are two fundamental properties associated with 1D metallic systems, which may be present in these MTBs. Firstly, 1D metallic lattices are expected to be unstable and undergo a charge density wave (CDW) transition, which is also known as a Peierls transition for 1D structures [92–96]. Secondly, electrons confined in 1D become a strongly correlated quantum liquid and it should obey a Tomonaga–Luttinger liquid behavior rather than the quasi single particle excitation behavior in a 2D or 3D metallic Fermi-liquid. Indeed evidence

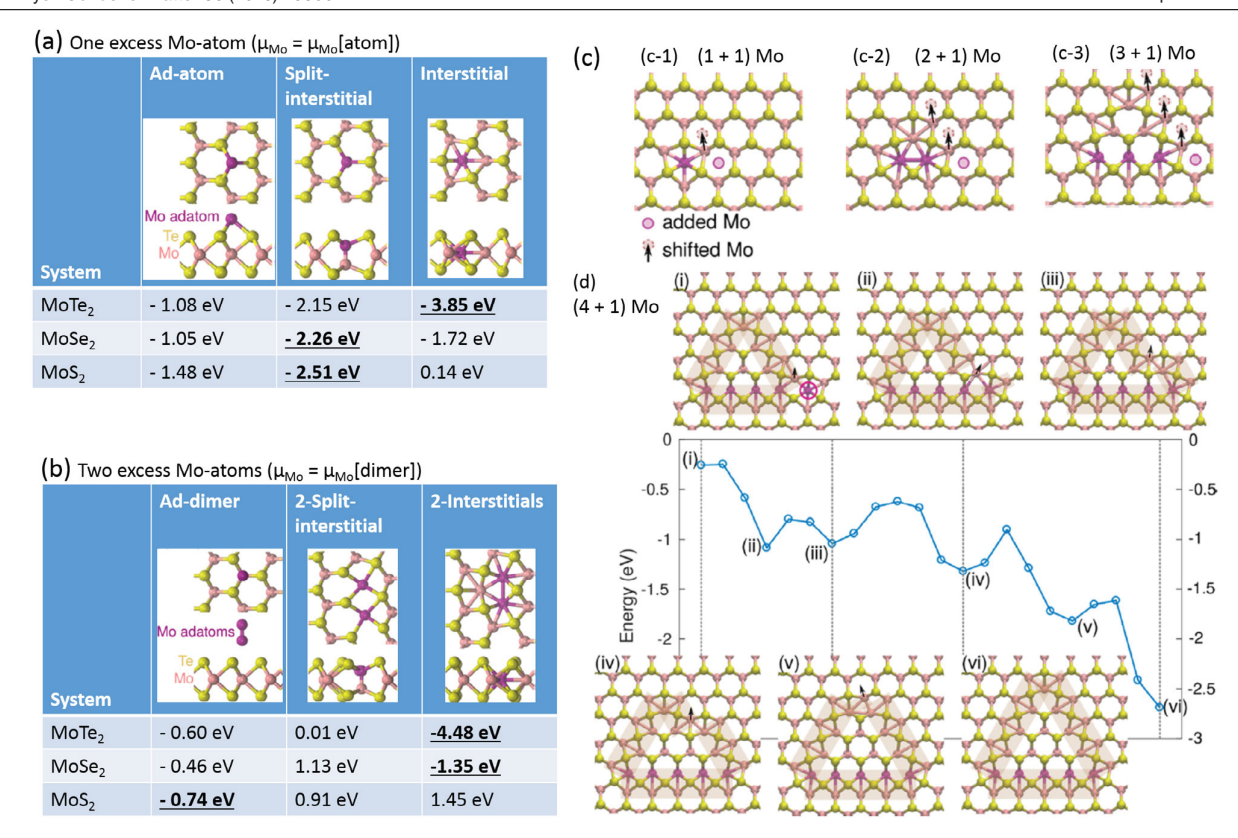


Figure 7. Energies for the incorporation of excess Mo into  $MoX_2$ . Energies of three configurations for a single excess Mo-atom and two excess Mo-atoms for  $MoTe_2$ ,  $MoSe_2$ , and  $MoS_2$  are shown in (a) and (b), respectively. The reference chemical potential is that of a free Mo-atom or Mo-dimer, respectively. For a two Mo-atoms it is energetically favored for two excess Mo-atoms to occupy neighboring interstitial sites for  $MoTe_2$  and  $MoSe_2$  while it is favored to have Mo-dimers adsorbed on  $MoSe_2$ . In (c) it is illustrated how addition of Mo-atoms can result in restructuring of the crystal to form a MTB-loop. In (d) it is shown that growth of the MTB loop by adding a Mo-atom is all energetically downhill in  $MoTe_2$ . Reprinted with permission from [86]. Copyright (2018) American Chemical Society.

for both expectations for 1D metals have been observed in MTBs of MoSe<sub>2</sub> and are discussed next.

#### 3.1. Charge density wave (Peierls) transition

A CDW transition is related to a Fermi-surface instability due to electron-phonon coupling and can be described by a Fermi-nesting condition. In 1D systems the Fermi-surface consists of two parallel lines in k-space separated by twice the Fermi-vector  $k_{\rm F}$  and thus exhibit perfect nesting conditions that allows translation of one Fermi-line onto the other with a single reciprocal wave vector q (nesting vector). This results in a freezing in of a phonon mode of  $q = 2 k_F$  and formation of a lattice distortion of  $2\pi/q$  in real space, which gives rise to a modulation in the charge density along the 1D lattice. The energy cost for the lattice distortion is compensated for by an opening of a small energy gap at the Fermi-level. Hallmarks for the formation of a CDW transition have been suggested to be observed in MTBs of MoSe2 and are summarized in figure 8. Most importantly a tripling of the periodicity along the MTBs has been observed in low temperature STM studies at 4K [97] and 120K [98] compared to room temperature studies as shown in figure 8(a). At room temperature the atomic periodicity is observed and the triple periodicity of the atomic lattice ( $d \approx 10 \text{ Å}$ ) may thus be interpreted as the periodicity of a CDW. The achievable high density of grain boundaries in MBE grown MoSe<sub>2</sub> on MoS<sub>2</sub> single crystal substrates allowed to experimentally study the k-space resolved electronic structure of such grain boundaries by ARPES as shown in figure 8(b). The Fermi-surface exhibits two parallel lines as expected for a 1D electron system, demonstrating perfect nesting conditions of the electronic structure of these MTBs. Moreover, the measured Fermi-vector  $k_{\rm F} = 0.30 \pm 0.02 \ {\rm A}^{-1}$  agrees with the real space periodicity, i.e.  $d \approx 10 \text{ Å} = \pi/k_{\text{F}} = 10.5 \pm 0.7 \text{ Å}$ . Finally, in another study [97], shown in figure 8(c), an energy gap has been reported by STS around the Fermi-level for MoSe<sub>2</sub>, which has been interpreted as a CDW gap. However, the gap size varied and an average gap value of 100 meV with a relatively large standard deviation of 40 meV was reported. Similar gaps have also been measured recently by Michely et al for 4 | 4E MTBs (like those shown in figure 4(b)) in MoS<sub>2</sub>. In this case, the measured gap was inversely proportional to the grain boundary length. With the lengths of the grain boundaries defined by the widths of the islands in which the grain boundaries were embedded. A gap dependence on the length of the grain boundary cannot be explained by just a CDW. A possible alternative explanation of the measured gap that is unrelated to a CDW is

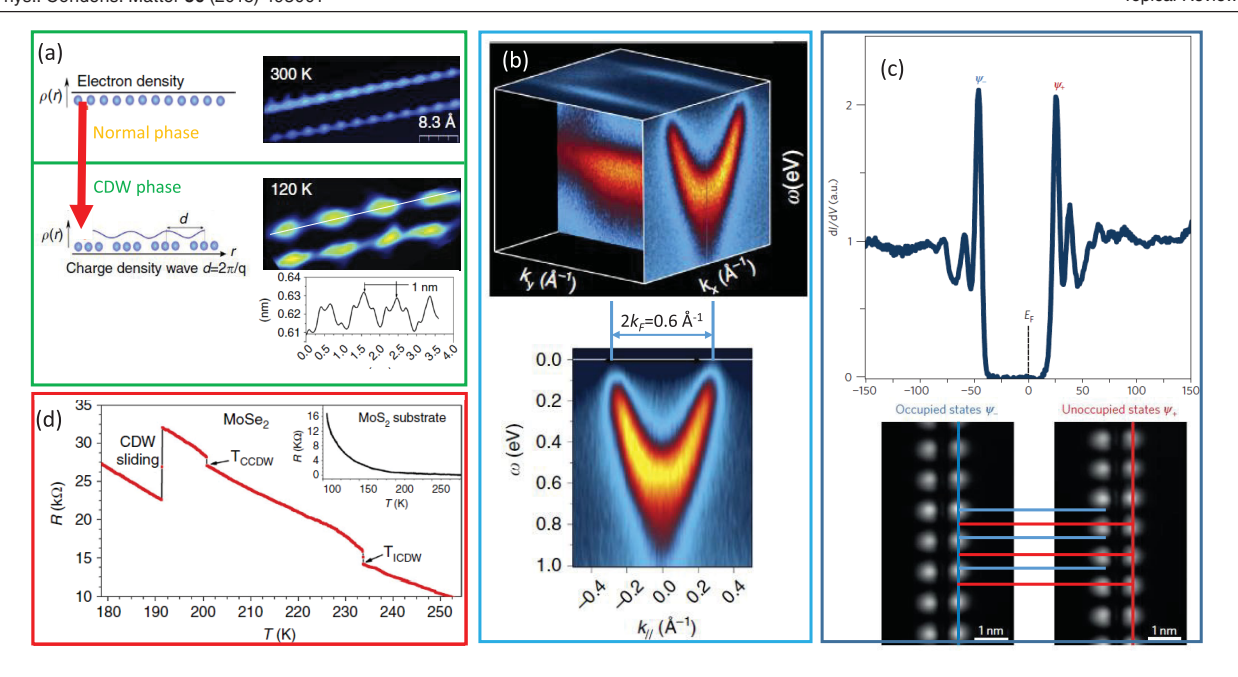


Figure 8. Evidence for charge density wave (Peierls) transition in MTBs in MoSe<sub>2</sub>. STM images, shown in (a) aquired at 300 K and 120 K show atomic corrugation and a corrugation of three times the lattice constant (~1 nm), respectively. ARPES studies of MTB networks of an MBE grown MoSe<sub>2</sub> layer on MoS<sub>2</sub> substrate show dispersing defect states with the linear Fermi surface of a 1D electron system (b). Although the photoemission intensity (density of states) is suppressed at the Fermi-level (see figure 9), there is still intensity at the Fermi-level and a Fermi-wave vector is measured to  $0.3 \text{ Å}^{-1}$ . Low temperature STS measurements on MTBs in MoSe<sub>2</sub> on graphene show a gap opening at the Fermi-level as shown in (c) and phase shift of the occupied and unoccupied states. Transport measurements on MTB networks shown in (d) indicate resistance jumps that are interpreted as incommensurate and commensurate CDW transitions. Also a sharp drop of the resistance is observed which has been suggested to be due to a CDW sliding transition. (a), (b) Reproduced from [98]. CC BY 4.0. (c) [97] (2016) (© 2018 Springer Nature Limited. All rights reserved). With permission of Springer. (d) Reproduced from [98].

that adding or removing electrons to a nano-object may cost some charging energy. This charging energy depends on the size (i.e. capacitance) of the object with more energy required for a small object. The minimum energy required to add (or remove) an electron may cause a charging gap in STS measurements. Such charging gaps may be an alternative explanation for the observed gaps in the metallic grain boundaries if they are sufficiently decoupled from the graphene substrates used in the STS studies. In addition quantum confinement effects in the short MTB segments under investigation may give rise to quantized energy levels of the electrons or the collective quantum liquid if modeled by a TLL (as discussed next). These quantum confinement effects may contribute to the observed gap. Thus the origin of the observed energy gap in STS remains an area of ongoing controversy. In general, charging gaps may also be observed in ARPES, but there may be several reasons why it has not been observed in the case for the data reported in [98]. First, the measurements were taken at room temperature where thermal excitations suppress charging; second, the measurements average over a large area and this may smear out any charging gaps; and third, the measurements were taken on a dense network of wires and thus the charging gap should be related to the capacitance of the entire network and not to that of an individual wire.

The limited length of the grain boundaries can also give rise of quantum confinement effects. Electron confinement in a particles-in-a-box was first suggested from dI/dV mapping with STM by Liu *et al* [78]. It has also been pointed out that the fundamental wavelength of such an electron confinement is given by the Fermi-wave vector and thus the three times periodicity observed in STM images may not be a consequence of a CDW but the electron confinement in MTBs with limited length. This controversy could be settled if longer MTBs could be observed with STM. However, to date, all STM studies have been made on fairly short segments that could exhibit significant quantum confinement effects.

While there continues to exist controversy if the STS and STM data indicate the presence of a CDW in these MTBs, simple transport measurements on grain boundary networks, shown in figure 8(d), appear to be consistent with CDW transitions. Temperature dependent 4-point resistance measurements on MBE-grown MoSe<sub>2</sub> on a MoS<sub>2</sub> substrates show two jumps in resistance at ~235 K and ~205 K. Such resistance increases are commonly observed in Peierls systems and are generally associated with an incommensurate and commensurate CDW transition. Furthermore, a precipitous drop in resistance is observed if a critical voltage is applied. This is also observed frequently in other Peierls systems and is associated with a CDW sliding transition [99, 100] Sliding transitions occur due to a de-pinning of the CDW from defects at a critical electric field (or applied potential). The challenge with these studies on MTB networks is that they average over the complex morphologies on a macroscopic scale and thus may not represent the properties of a single MTB.

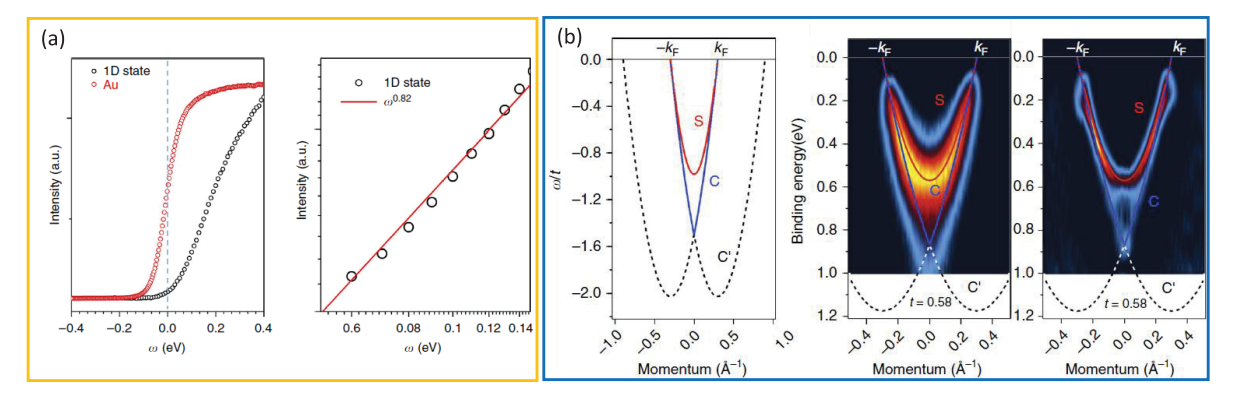


Figure 9. Evidence for TLL in MTB networks of MoSe<sub>2</sub>. (a) The suppression of the density of states close to the Fermi-level is observed from the integration of the photoemission intensity in the momentum range from  $-0.4 \, \text{Å}^{-1}$  to  $0.4 \, \text{Å}^{-1}$  of the photoemission data shown in (b), and compared to the Fermi-ledge of a Fermi-liquid material (here gold). The density of states close to the Fermi level can be expressed by a power law behavior as shown by the logarithmic plot with an exponent of ~0.8. Such an exponent is indicative of strong electron interactions and the 1D electron removal spectra may be modeled by 1D Hubbard model with appropriate finite range interactions, as shown in (b). Only the measured Fermi-wave vector and the exponent of the power law suppression of the density of states are parameters in the model. The spin-(S) and charge- (C) excitation branches are indicated in (b), where the C' branch has zero spectral intensity. These modeled spectral branches agree well with the experimental data as shown on the raw data and the second-derivative of the raw data. Reproduced from [98]. CC BY 4.0.

To conclude this sub-section, it is reasonable to expect a CDW transition in this system. From the 1D Fermi surface a CDW instability may be expected. However, the STM and STS data may also be interpreted by alternative phenomena related to the limited length of the MTBs studied, so far.

#### 3.2. Tomonaga-Luttinger liquid (TLL) behavior

While electrons in 2D- or 3D-metals can be described effectively by single particle excitations in a Fermi-liquid approximation, such single quasiparticle excitation mechanism breaks down in 1D metals. In 1D-metals electrons become a strongly correlated quantum liquid, known as a TLL [101-107]. In TLL separate excitations of their charge and spin degrees of freedom are observed. This is commonly known as spin-charge separation in 1D systems, giving rise to branches with distinct dispersions in electron removal spectra such as photoemission. A description of TLL theory is beyond the scope of this review and we focus on the experimental evidence for the existence of TLL in MTBs. It is noteworthy that clear experimental evidence of TLL is rare and often controversial [108-110]. ARPES and STM/STS are suitable tools for determining TLL properties. Prediction of TLL are that the density of states are suppressed at the Fermi-level, i.e. instead of exhibiting a Fermi-Dirac distribution, the density of states should follow a power law behavior for both the energy dependence as well as the temperature dependence. The exponent in the power law is related to the electron interaction strength of the TLL. ARPES measurements on MTB networks [98] indeed showed a power law suppression of the density of states with a power law exponent between 0.75 and 0.8. Such exponents indicate electrons with finite range interactions and thus need to be modeled by a 1D Hubbard model that include such finite range interactions [98]. Such models predict two spectral branch lines in electron removal spectra corresponding to spin and charge excitations.

The calculated branch lines agree very well with the experimental data obtained for MTB networks as shown in figure 9. The broad ARPES spectra obtained at RT, i.e. above any potential CDW transition, is too broad to be fit with a single band and energy distribution curves clearly indicate the presence of at least two peaks. The second derivative of the spectral intensity, shown in figure 9(b), also indicates two cusp-lines in the spectra. These cusps are very well reproduced by the prediction of the 1D Hubbard model with finite range interactions that only uses the measured Fermi-wave vector and the power law exponent of the spectral intensity at the Fermi-level as input parameters. Thus the ARPES data are well described by a TLL behavior. Further evidence for a TLL in MTBs come from recent dI/dV mapping of MTBs in MoS<sub>2</sub> by the Michely group. These results have not yet appeared in peer-reviewed journals, but were presented at conferences [111, 112]. Their data can only be explained by a quantum confinement of a TLL. In their simulations they also can reproduce the above mentioned gap opening at the Fermi-level due to limited size effects without assuming a CDW. Therefore, it seems that two independent studies indicate that metallic MTBs embedded in semiconducting TMDs indeed host a TLL.

# 4. Potential applications: chemical properties, metallization, surface functionalization and pinning of metal clusters

For most electronic applications defects and grain boundaries are undesirable, with gap states causing charge carrier trapping and may explain variable range hopping in MBE grown MoSe<sub>2</sub> and MoTe<sub>2</sub> [65, 66], or act as non-radiative electronhole recombination sites in opto-electronic applications [67]. Therefore, avoiding grain boundaries is critical [36]. The identification of the formation of MTB loops in MoSe<sub>2</sub> and MoTe<sub>2</sub> by incorporation of Mo makes it difficult to avoid such defects in MBE-grown films. It appears that layers grown by

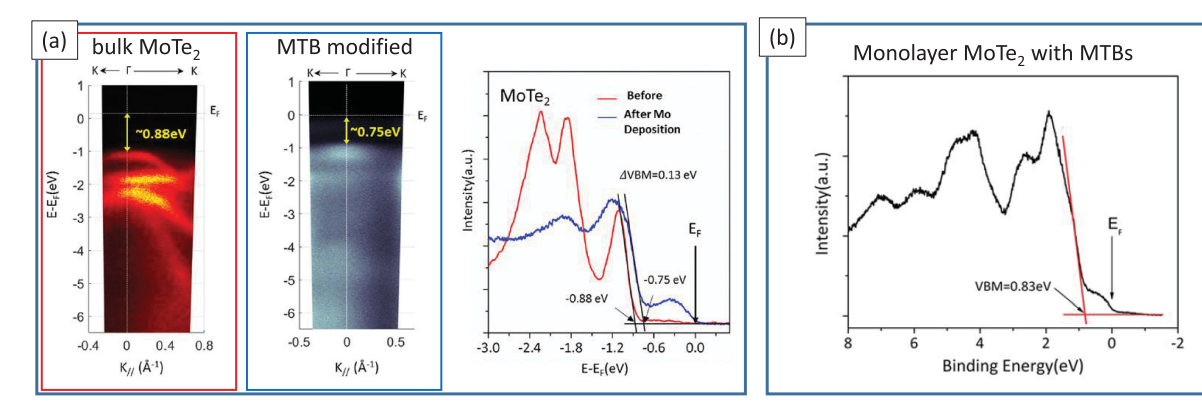
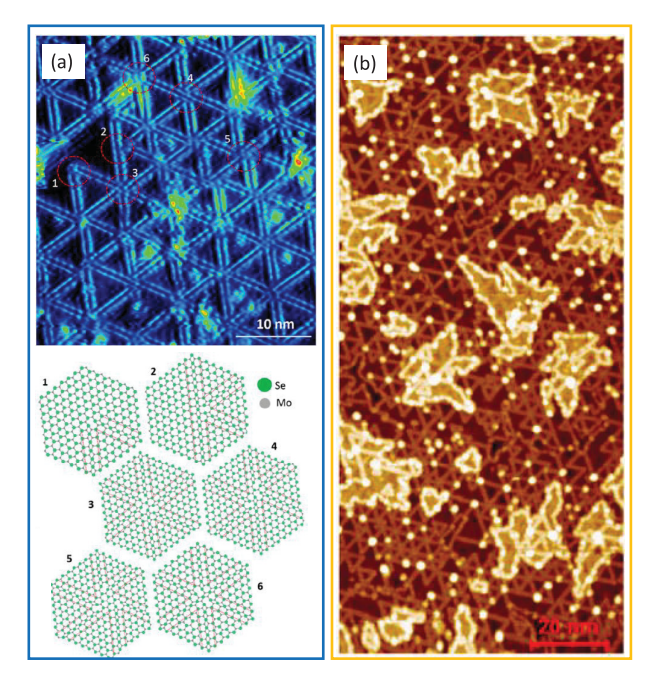


Figure 10. Determination of charge neutrality level of MTB induced gap states in MoTe<sub>2</sub> by valence band photoemission spectroscopy. ARPES measurement of a bulk MoTe<sub>2</sub> single crystal before and after modification of the surface with MTB networks is shown in (a). From the energy distribution curves taken at the Γ-point an upward shift of the VBM by ~130 meV to 750 meV below the Fermi-level is observed after modification with MTBs. Also the MTB-induced band gap states are clearly seen. On monolayer MoTe<sub>2</sub> with a high density of MTBs the VBM is measured at ~830 meV below the Fermi-level as is shown in (b) from UPS measurements. (a) Reprinted with permission from [86]. Copyright (2018) American Chemical Society. (b) Reprinted from [83], with the permission of AIP Publishing.

different groups may exhibit different defect concentrations. While currently there exist no systematic growth studies on how to avoid the formation of MTBs in MBE growth entirely, it appears that defect concentrations are higher for very low growth rates and some reports suggests that MTB concentrations may be reduced by post-growth annealing in Se [38]. For growth of MoS<sub>2</sub>, DFT and experiments discussed in section 2 indicate that MTBs do not form by excess Mo-incorporation into the lattice, but twin grains may still form due to coalescence of inversion grains. If the symmetry of the substrate is higher (e.g. graphene with 6-fold symmetry) than the 3-fold symmetry of MoS<sub>2</sub>, then formation of twins is unavoidable. However, studies for growth on 3-fold symmetric hexagonal substrates (e.g. on Au(111)) have shown that by tuning the growth conditions twin grain formation can be suppressed [76]. Thus it appears possible to grow MTB free MoS<sub>2</sub> monolayers on a macroscopic scale on suitable substrates and growth conditions.

#### 4.1. Metal contacts

The metallic properties of MTBs and their easy formation by incorporating excess Mo into the lattice of MoSe<sub>2</sub> and MoTe<sub>2</sub>, may make these crystal modifications useful in applications. Metallization of transition metal dichalcogenides has been explored as an approach to make good electrical contacts to these layered materials. For instance, the 2H-semicondcuting to 1T-metallic phase transition in MoS2 has been studied for this purpose. Such phase transitions may be induced by electron doping (e.g. by Li adsorption) [113] or in the case of MoTe<sub>2</sub> a transition from 2H to its 1T' phase may be induced by temperature treatment [114]. Incorporation of excess Mo, may be an alternative approach for metallizing MoSe<sub>2</sub> and MoTe<sub>2</sub> by formation of MTB networks. To be practical, contacts need to be fabricated at predefined positions on a monolayer wafer of MoSe<sub>2</sub> or MoTe<sub>2</sub>. The process of incorporation of excess Mo into an initially defect-free wafer allows to use, for example, a shadow mask for locally depositing Mo onto



**Figure 11.** MTB networks for metal cluster nucleation. Different MTB intersection configurations are illustrated in (a). Nucleation of Au-clusters at MTB intersections is observed in (b) for vapor deposited gold at room temperature on a  $MoSe_2$  MTB network. Reprinted with permission from [79]. Copyright (2017) American Chemical Society.

the surface and to modify this region selectively with MTB networks.

Fermi-level pinning at semiconductor surfaces due to formation of surface reconstructions with high density of states in the semiconductor bulk gap is a well-known phenomenon [115]. The formation of dense metallic line defect networks described here is very similar to metallic surface reconstructions in semiconductors. The line defects exhibit a high density of states within the band gap of 2H-MoX<sub>2</sub>, which pins the Fermi-level to the charge neutrality point of the defect states

**Figure 12.** Mirror twin grain boundaries in CVD grown MoS<sub>2</sub>. (a) Bright field TEM image of 6-pointed MoS<sub>2</sub> island with inset diffraction pattern. On the right the dark-field TEM image is shown corresponding to the diffraction spot marked with orange circle. The dark-filed image indicates that the island contains several mirror twin grains and thus micrometer long MTBs. (b) Back-gated transport measurements parallel and perpendicular to a MTB grain boundary (GB) of a CVD-grown MoS<sub>2</sub> on a Si/SiO<sub>2</sub> substrate at room temperature. The conductance along the grain boundary is always higher, however, it is not obvious if the change in conductance as a function of gate voltage is an intrinsic response of the MTB or is related to the field effect in the MoS<sub>2</sub>. [120] (2013) (© 2018 Springer Nature Limited. All rights reserved). With permission of Springer.

(i.e. the energy level for which the defect remains uncharged). This is identical to the Fermi-level being pinned to charge neutrality points in semiconductor surface reconstruction. The position of these neutrality points are defined with respect to the semiconductor band edges and thus the Fermi-level in such systems is fixed (or pinned) within the band gap of the semiconductor. ARPES measurements, shown in figure 10(a) on MoTe<sub>2</sub> single crystals before and after modification of the surface with MTB networks, show that the valence band maximum (VBM) shifts up by 130 meV towards the Fermilevel for this particular doping-level in the single crystal after formation of MTB networks. Consequently, the VBM was measured at 750 meV below the Fermi-level for bulk MoTe<sub>2</sub> system. A slightly different value of 830 meV was measured for the VBM for MTB modified monolayer MoTe<sub>2</sub> grown on MoS<sub>2</sub> substrates, as shown in figure 10(b). This ~80 meV difference may be related to variations of the band gap in monoversus multi-layer samples due to interlayer interactions. It can be also seen in figure 10 that the band structure of MoTe<sub>2</sub> becomes broadened and smeared out upon formation of MTB networks. Such behavior is expected from the disruption of the crystal structure by the MTBs.

The low barriers for incorporation of Mo into MoSe<sub>2</sub> and MoTe<sub>2</sub> also raises the question if other transition metals may be incorporated into these materials. This may have implications for metal/MoX<sub>2</sub> interfaces. If metals are deposited to MoSe<sub>2</sub> or MoTe<sub>2</sub> then depending on the diffusion barriers and deposition temperatures the metal may diffuse into MoX<sub>2</sub>. For instance in [86] it was shown that Ti, a common metal to increase adhesion of metal contacts, will incorporate into MoTe<sub>2</sub>. Such incorporation of metals into the MX<sub>2</sub> lattice are likely to result in defect states that will modify the metal contacts. Thus this mechanism of metal intermixing with TMDCs needs to be taken into consideration when making metal contacts, which so far have only been modeled as weakly or strongly interacting metals but without possibility of metal incorporation [116]. As shown above for Mo-intermixing, the degree of intermixing will depend not just on the metal but also on the TMDC.

#### 4.2. Metal decoration/sintering

Defect free TMDCs, like other 2D materials, lack any dangling bonds at the surface and are therefore fairly inert. Therefore metals deposited on such surfaces usually are not anchored well but agglomerate into larger clusters. Thus pristine TMDCs are not good support materials for example for metal catalysts that would sinter into large agglomerates. Defects at surfaces can act as nucleation sites for metals and pin metal clusters to suppress sintering. In figure 6, it can be seen that Mo-clusters form preferentially at corners of intersecting MTBs on MoSe<sub>2</sub>, suggesting that these are sites with higher adsorption energies for metal atoms. Thus in this process the deposited metal first creates MTBs that than form sites for anchoring metals. Consequently, this may be described as a self-induced formation of metal adsorption sites that operates on MoSe<sub>2</sub> and MoTe<sub>2</sub> due to its metal induced formation of MTB networks. It appears that the MTBs themselves do not exhibit a significantly higher metal adsorption energy, but all the metal clusters form at points where MTBs intersect. This metal decoration has been further studied by gold deposition on MTB networks on MoSe<sub>2</sub> monolayers, as shown in figure 11 [79]. As illustrated in figure 11(a) the intersections between MTBs can have different local coordinations with varying degrees of unsaturated bonds. The ball-and-stick models shown in figure 11(a) are only suggestions of possible configurations based on the experimental offsets of MTBs observed in the STM images. In figure 11(b) small amounts of Au have been vapor deposited on such networks. It is obvious from the STM images that the Au-clusters only nucleate at MTB intersections. It is, however, also apparent that Au-clusters are not observed at all intersections. The study is not conclusive if the nucleation of Au-clusters at intersections is stochastic or if certain configurations of intersections have a higher metal nucleation probability. Thus further systematic studies are required to identify MTB intersection configurations with strong metal adsorption. In addition to adsorption of metals, it can be envisioned that these defect sites are also reactive for adsorbing molecules and thus present sites that can be used to functionalize these surfaces with molecular ligands.

#### 4.3. Electrocatalysis

Metallic edge states in MoS2 have been identified as important catalytic sites for electrochemical applications of TMDCs, for example for hydrogen evolution reaction (HER) catalysis [117]. The metastable 1T phases have also been identified as being more catalytically active compared to the mostly inactive 2H phases [118, 119]. Recently, it has been shown that MBE grown mono- to few layers of MoSe<sub>2</sub>, MoTe<sub>2</sub> and their solid solutions also exhibit increased electrocatalytic properties for HER [68]. These increased catalytic activity compared to pristine MoSe<sub>2</sub> or MoTe<sub>2</sub> has been attributed to the MTB networks in these materials. While tellurium is a rare and expensive element and thus MoTe<sub>2</sub> may not be an attractive material for replacing traditional Pt-catalysts, MoSe<sub>2</sub> may be a more reasonable material to consider from a cost standpoint. Thus the modification of MoSe<sub>2</sub> electrodes with MTB networks appears to be a potentially interesting approach for boosting its electrocatalytic activity. Further investigations are needed to explore the feasibility of MoSe2 and the importance of MTBs in electrocatalysis.

#### 5. Conclusions and outlook

MTBs are metallic line defects in TMDCs, exhibiting dispersing bands and thus making them exciting materials for probing electronic properties in 1D. So far these properties have been mainly probed by scanning probe microscopy and ARPES on short segments of MTBs. Because of the limited length of the MTBs, either in network structures or in small MoS<sub>2</sub>-islands, quantum confinement of the electrons in this 1D-potential box, may play an important role for describing their properties. In addition, the small size may give rise to charging effects in STS. Thus while experimental observations are consistent between different groups there remain some controversies of their interpretations such as Peierls transition versus confined electronic states for the observed periodicity in STM images and, moreover, if the band gap opening is due to Peierls transition or charging and TLL behavior. Most of the controversy could be resolved by studying longer MTBs. The MTBs studied by STM have been studied on samples grown in UHV by MBE or MBE related methods to maintain clean environments. In CVD grown samples much larger grains can be obtained and twinned grains are quite common in e.g. MoS<sub>2</sub> as shown in figure 12 [120]. TEM has identified the MTBs in such grain boundaries, however, the maximum defect-free length of the MTBs has not been reported. Such extended MTBs could be single truly 1D wires. Locating them with an STM tip may be challenging but doable in instruments that combine STMs with SEMs and this may be a worthwhile endeavor to resolve the importance of limited size effects in the STM characterization of MTBs. Moreover, such extended MTBs may allow transport measurements on a single MTB

rather than the previously reported measurements on MTB networks [79], which are an averaging over complex structures. Contacting and measuring resistance of an MTB has been attempted before as shown in figure 12(b), but unfortunately no temperature dependent studies were reported.

In MoS<sub>2</sub> the formation of MTBs appears to be exclusively observed by merging of grains with twin orientations. Interestingly in MoSe<sub>2</sub> and MoTe<sub>2</sub> MTB-loops can form by incorporation of excess Mo into the lattice. The excess Mo then reorganizes in MTBs and can form dense networks, which modifies the materials properties. Thus this is an approach of introducing new functionalities in these materials and may be exploited for metallizing certain TMDCs to make better electrical contacts to 2D materials or induce catalytic properties. These potential applications will need further development. Another potentially interesting aspect is the incorporation of other transition metals into MoSe<sub>2</sub> and MoTe<sub>2</sub> not just Mo. These dopants may allow to add further functionalities into these materials. However, which transition metals like to incorporate into MoX2 and if such hetero-interstitials would also like to undergo site-exchange with lattice Mo and cause re-organization into MTB networks still needs to be studied.

Finally, most studies of MTBs have been done on MoX<sub>2</sub> because initial work on TMDCs focused on MoS<sub>2</sub> and because of the observation of MTB networks in MBE-grown MoSe<sub>2</sub> and MoTe<sub>2</sub>. The formation of dense MTB networks in MBE-grown MoSe<sub>2</sub> or MoTe<sub>2</sub> is primarily a consequence of the easy incorporation of excess Mo into these materials. This mechanism for the formation of MTB loops by incorporation of excess transition metals is, however, a specific property for MoSe<sub>2</sub> and MoTe<sub>2</sub>, only. Consequently, other TMDCs will not form high density MTB networks. Nevertheless, coalescence of 60° rotated grains during growth will always result in MTBs. Based on the exciting properties of MTBs in MoX<sub>2</sub> studying MTBs in other TMDCs may enable to increase our understanding of the physics of 1D systems.

#### Acknowledgment

The author acknowledges support from the National Science Foundation under awards ECCS-1608654, DMR-1701390, and CHE-1801199.

#### **ORCID iDs**

Matthias Batzill https://orcid.org/0000-0001-8984-8427

#### References

- [1] Lauritsen J V, Kibsgaard J, Helveg S, Topsøe H, Clausen B S, Lægsgaard E and Besenbacher F 2007 Nat. Nanotechnol. 2,53–8
- [2] Schweiger H, Raybaud P, Kresse G and Toulhoat H 2002 J. Catal. 207 76–87
- [3] Kibsgaard J, Lauritsen J V, Lægsgaard E, Clausen B S, Topsøe H and Besenbacher F 2006 J. Am. Chem. Soc. 128 13950–8

- [4] Chung D Y, Yoo J M, Park S, Jung G Y, Kang J S, Ahn C Y, Kwak S K and Sung Y-E 2018 Small 14 1802191
- [5] Bruix A, Füchtbauer H G, Tuxen A K, Walton A S, Andersen M, Porsgaard S, Besenbacher F, Hammer B and Lauritsen J V 2015 ACS Nano 9 9322–30
- [6] Lauritsen J V, Nyberg M, Vang R T, Bollinger M V, Clausen B S, Topsøe H, Jacobsen K W, Lægsgaard E, Nørskov J K and Besenbacher F 2003 Nanotechnol. 14 385–9
- [7] Geim A K and Grigorieva I V 2013 Van der Waals heterostructures *Nature* 499 419–25
- [8] Dean C R et al 2013 Nature 497 598-602
- [9] Ponomarenko L A et al 2013 Nature 497 594-7
- [10] Ma Q et al 2016 Nat. Phys. 12 455
- [11] Liu C H, Clark G, Fryett T, Wu S F, Zheng J J, Hatami F, Xu X D and Majumdar A 2017 Nano Lett. 17 200–5
- [12] Vu Q A et al 2017 Nano Lett. 17 453-9
- [13] Wang F, Wang Z, Xu K, Wang F, Wang Q, Huang Y, Yin L and He J 2015 Nano Lett. 15 7558–66
- [14] Padilha J E, Fazzio A and da Silva A J R 2015 Phys. Rev. Lett. 114 066803
- [15] Huo N J, Kang J, Wei Z M, Li S S, Li J B and Wei S H 2014 Adv. Funct. Mater. 24 7025–31
- [16] Lopez-Sanchez O, Llado E A, Koman V, Morral A F I, Radenovic A and Kis A 2014 ACS Nano 8 3042–8
- [17] Schaibley J R, Rivera P, Yu H Y, Seyler K L, Yan J Q, Mandrus D G, Taniguchi T, Watanabe K, Yao W and Xu X D 2016 Nat. Commun. 7 13747
- [18] Chen H L et al 2016 Nat. Commun. 7 12512
- [19] Peng B, Yu G N, Liu X F, Liu B, Liang X, Bi L, Deng L I, Sum T C and Loh K P 2016 2D Mater. 3 025020
- [20] Rivera P, Seyler K L, Yu H Y, Schaibley J R, Yan J Q, Mandrus D G, Yao W and Xu X D 2016 Science 351 688–91
- [21] Rivera P et al 2015 Nat. Commun. 6 6242
- [22] Fang H et al 2014 Proc. Natl Acad. Sci. USA 111 6198-202
- [23] Novoselov K S, Mishchenko A, Carvalho A and Castro Neto A H 2016 Science 353 461
- [24] Jariwala D, Sangwan V K, Lauhon L J, Marks T J and Hersam M C 2014 ACS Nano 8 1102–20
- [25] Samad L, Bladow S M, Ding Q, Zhuo J Q, Jacobberger R M, Arnold M S and Jin S 2016 ACS Nano 10 7039–46
- [26] Choudhary N, Park J, Hwang J Y, Chung H S, Dumas K H, Khondaker S I, Choi W B and Jung Y 2016 Sci. Rep. 6 25456
- [27] Zhang Q, Chen Y X, Zhang C D, Pan C R, Chou M Y, Zeng C G and Shih C K 2016 Nat. Commun. 7 13843
- [28] Zhao M, Liu M M, Dong Y Q, Zou C, Yang K Q, Yang Y, Zhang L J and Huang S M 2016 J. Mater. Chem. C 4 10215–22
- [29] Ben Aziza Z, Henck H, Pierucci D, Silly M G, Lhuillier E, Patriarche G, Sirotti F, Eddrief M and Ouerghi A 2016 ACS Nano 10 9679–86
- [30] Aretouli K E, Tsoutsou D, Tsipas P, Marquez-Velasco J, Giamini S A, Kelaidis N, Psycharis V and Dimoulas A 2016 ACS Appl. Mater. Interfaces 8 23222–9
- [31] Li X F et al 2016 Sci. Adv. 2 e1501882
- [32] Tsoutsou D, Aretouli K E, Tsipas P, Marquez-Velasco J, Xenogiannopoulou E, Kelaidis N, Giamini S A and Dimoulas A 2016 ACS Appl. Mater. Interfaces 8 1836–41
- [33] Liu X L, Balla I, Bergeron H, Campbell G P, Bedzyk M J and Hersam M C 2016 ACS Nano 10 1067–75
- [34] Coy Diaz H, Chaghi R, Ma Y and Batzill M 2015 2D Mater. 2 044010
- [35] Li X F et al 2015 ACS Nano 9 8078-88
- [36] Vishwanath S et al 2015 2D Mater. 2 024007
- [37] Miwa J A, Dendzik M, Gronborg S S, Bianchi M, Lauritsen J V, Hofmann P and Ulstrup S 2015 ACS Nano 9 6502–10

- [38] Jiao L et al 2015 New J. Phys. 17 053023
- [39] Yuan X et al 2015 Nano Lett. 15 3571-7
- [40] Aretouli K E, Tsipas P, Tsoutsou D, Marquez-Velasco J, Xenogiannopoulou E, Giamini S A, Vassalou E, Kelaidis N and Dimoulas A 2015 Appl. Phys. Lett. 106 143105
- [41] Yan A, Velasco J Jr, Kahn S, Watanabe K, Taniguchi T, Wang F, Crommie M F and Zettl A 2015 Nano Lett. 15 6324–31
- [42] Lv R, Robinson J A, Schaak R E, Sun D, Sun Y, Mallouk T E and Terrones M 2015 Acc. Chem. Res. 48 56–64
- [43] Robinson J A 2016 ACS Nano 10 42-5
- [44] Walsh L A and Hinkle C L 2017 Appl. Mater. Today 9 504–15
- [45] Bonilla M et al 2018 Nat. Nanotechnol. 13 289-93
- [46] Kolekar S, Bonilla M, Ma Y, Coy Diaz H and Batzill M 2017 2D Mater. 5 015006
- [47] Koma A 1999 J. Cryst. Growth 201 236
- [48] Koma A 1992 Thin Solid Films 216 72-6
- [49] Ohuchi F S, Parkinson B A, Ueno K and Koma A 1990 J. Appl. Phys. 68 2166–75
- [50] Ueno K, Takeda N, Sasaki K and Koma A 1997 Appl. Surf. Sci. 113 38–42
- [51] Ohuchi F S, Shimada T, Parkinson B A, Ueno K and Koma A 1991 J. Cryst. Growth 111 1033–7
- [52] Schlaf R, Tiefenbacher S, Lang O, Pettenkofer C and Jaegermann W 1994 Surf. Sci. 303 L343–7
- [53] Yamada H, Ueno K and Koma A 1996 Japan. J. Appl. Phys. 35 L568–70
- [54] Lang O, Schlaf R, Tomm Y, Pettenkofer C and Jaegermann W 1994 J. Appl. Phys. 75 7805–13
- [55] Schlaf R, Lang O, Pettenkofer C and Jaegermann W 1999 J. Appl. Phys. 85 2732–53
- [56] Lang O, Klein A, Pettenkofer C, Jaegermann W and Chevy A 1996 J. Appl. Phys. 80 3817–21
- [57] Schlaf R, Pettenkofer C and Jaegermann W 1999 J. Appl. Phys. 85 6550–6
- [58] Kreis C, Traving M, Adelung R, Kipp L and Skibowski M 2000 Appl. Surf. Sci. 166 17–22
- [59] Kreis C, Werth S, Adelung R, Kipp L, Skibowski M, Voss D, Krueger P, Mazur A and Pollmann J 2002 Phys. Rev. B 65 153314
- [60] Tiefenbacher S, Pettenkofer C and Jaegermann W 2000 Surf. Sci. 450 181–90
- [61] Klein A, Tiefenbacher S, Eyert V, Pettenkofer C and Jaergermann W 2001 Phys. Rev. B 64 205416
- [62] Ugeda M M et al 2014 Nat. Mater. 13 1091-5
- [63] Bruix A et al 2016 Phys. Rev. B 93 165422
- [64] Coy Diaz H, Ma Y, Kolekar S, Avila J, Chen C, Asensio M C and Batzill M 2017 2D Mater. 4 025094
- [65] Roy A, Movva H C P, Satpati B, Kim K, Dey R, Rai A, Pramanik T, Guchhait S, Tutuc E and Banerjee S K 2018 ACS Appl. Mater. Interfaces 8 7396–402
- [66] Chen M-W et al 2017 ACS Nano 11 6355-61
- [67] Chen K, Roy A, Rai A, Movva H C P, Meng X, He F, Banerjee S K and Wang Y 2018 APL Mater. 6 056103
- [68] Kosmala T, Coy Diaz H, Komsa H-P, Ma Y, Krasheninnikov A V, Batzill M and Agnoli S 2018 Adv. Energy Mater. 8 1800031
- [69] Zhou W et al 2013 Nano Lett. 13 2615-22
- [70] Lin J, Pantelides S T and Zhou W 2015 ACS Nano 9 5189–97
- [71] Lehtinen O et al 2015 ACS Nano 9 3274-83
- [72] Komsa H-P and Krasheninnikov A V 2017 Adv. Electron. Mater. 3 1600468
- [73] Lin Y-C et al 2015 Nat. Commun. 6 6736
- [74] Zhao X, Kotakoski J, Meyer J C, Sutter E, Sutter P, Krasheninnikov A V, Kaiser U and Zhou W 2017 MRS Bull. 42 667–76
- [75] Hall J, Pielić B, Murray C, Jolie W, Wekking T, Busse C, Kralj M and Michely T 2018 2D Mater. 5 025005

- [76] Bana H et al 2018 2D Mater. 5 035012
- [77] Murata H and Koma A 1999 Phys. Rev. B 59 10327-34
- [78] Liu H et al 2014 Phys. Rev. Lett. 113 066105
- [79] Ma Y, Kolekar S, Coy Diaz H, Aprojanz J, Miccoli I, Tegenkamp C and Batzill M 2017 ACS Nano 11 5130–9
- [80] Hong J et al 2017 Nano Lett. 17 6653-60
- [81] Dau M T 2018 ACS Nano 12 2319-31
- [82] Liu H, Zheng H, Yang F, Jiao L, Chen J, Ho W, Gao C, Jia J and Xie M 2015 ACS Nano 9 6619–25
- [83] Coy Diaz H, Ma Y, Chaghi R and Batzill M 2016 Appl. Phys. Lett. 108 191606
- [84] Yu Y, Wang G, Qin S, Wu N, Wang Z, He K and Zhang X-A 2017 Carbon 115 526
- [85] Chen J, Wang G, Tang Y, Tian H, Xu J, Dai X, Xu H, Jia J, Ho W and Xie M 2017 ACS Nano 11 3282–8
- [86] Coelho P M, Komsa H-P, Coy Diaz H, Ma Y, Krasheninnikov A V and Batzill M 2018 ACS Nano 12 3975–84
- [87] Zhu H, Wang Q, Cheng L, Addou R, Kim J, Kim M J and Wallace R M 2017 ACS Nano 11 11005–14
- [88] Arif A F, Balgis R, Ogi T, Iskandar F, Kinoshita A, Nakamura K and Okuyama K 2017 Sci. Rep. 7 3646
- [89] Zou X, Liu Y and Yakobson B I 2013 Nano Lett. 13 253-8
- [90] Gibertini M and Marzari N 2015 *Nano Lett.* **15** 6229–38
- [91] Lahiri J, Lin Y, Bozkurt P, Oleynik I I and Batzill M 2010 Nat. Nanotechno. 5 326–9
- [92] Heeger A J, Kivelson S, Schrieffer J R and Su W-P 1988 Rev. Mod. Phys. 60 781–850
- [93] Yeom H W et al 1999 Phys. Rev. Lett. 82 4898–901
- [94] Jérome D 2004 Chem. Rev. 104 5565-91
- [95] Shin J S, Ryang K-D and Yeom H W 2012 Phys. Rev. B 85 073401
- [96] Cheon S, Kim T-H, Lee S-H and Yeom H W 2015 Science 350 182–5
- [97] Barja S et al 2016 Nat. Phys. 12 751-6
- [98] Ma Y et al 2017 Nat. Commun. 8 14231
- [99] Thorne R E 1996 Phys. Today 49 42-7
- [100] Mantel O C, Bal C A W, Langezaal C, Dekker C and van der Zant H S J 1999 Phys. Rev. B 60 5287–94

- [101] Voit J 1995 Rep. Prog. Phys. 58 977-1116
- [102] Haldane F D M 1981 J. Phys. C: Solid State Phys. 14 2585–609
- [103] Imambekov A, Schmidt T L and Glazman L I 2012 Rev. Mod. Phys. 84 1253–306
- [104] Segovia P, Purdie D, Hengsberger M and Baer Y 1999 Nature 402 504–7
- [105] Claessen R et al 2002 Phys. Rev. Lett. 88 096402
- [106] Sing M et al 2003 Phys. Rev. B 68 125111
- [107] Ishii H et al 2003 Nature 426 540-4
- [108] Losio R et al 2001 Phys. Rev. Lett. 86 4632-6
- [109] Ahn J R, Yeom H W, Yoon H S and Lyo I W 2003 *Phys. Rev. Lett.* **91** 196403
- [110] Weitering H 2011 Nat. Phys. 7 744–5
- [111] Weiß P, Jolie W, Murray C, Hall J, Krasheninnikov A, Komsa H-P, Busse C, Michely T and Rosch A 2018 Spectral signatures of spin-charge separation on MoS<sub>2</sub> mirror twin boundaries *Verhandlungen der Deutschen Physikalischen Gesellschaft (Berlin, 13 March 2018)* p O 50.4 (www.dpg-verhandlungen.de/year/2018/conference/berlin/part/o/session/50/contribution/4)
- [112] Jolie W et al 2018 Verhandlungen der Deutschen Physikalischen Gesellschaft (Berlin, 15 March 2018) p O 99.4 (www.dpg-verhandlungen.de/year/2018/ conference/berlin/part/o/session/99/contribution/4)
- [113] Kappera R, Voiry D, Yalcin S E, Branch B, Gupta G, Mohite A D and Chhowalla M 2014 Nat. Mater. 13 1128–34
- [114] Cho S et al 2015 Science 349 625-8
- [115] Lüth H 2010 Solid Surfaces, Interfaces, and Thin Films 5th edn (Heidelberg: Springer)
- [116] Allain A, Kang J, Banerjee K and Kis A 2015 *Nat. Mater.* 14 1195–205
- [117] Jaramillo T F, Jorgensen K P, Bonde J, Nielsen J H, Horch S and Chorkendorff I 2007 Science 317 100–2
- [118] Lukowski M A et al 2013 J. Am. Chem. Soc. **135** 10274–7
- [119] Geng X et al 2016 Nat. Commun. 7 10672
- [120] Van der Zande A M et al 2013 Nat. Mater. 12 554-61